JACS
JOURNAL OF THE AMERICAN CHEMICAL SOCIETY
Article
pubs.acs.org/JACS

Delocalization-to-Localization Charge Transition in Diferrocenyl-Oligothienylene-Vinylene Molecular Wires as a Function of the Size by Raman Spectroscopy

Sandra Rodríguez González,[†] M. Carmen Ruiz Delgado,[†] Rubén Caballero,[‡] Pilar De la Cruz,[‡] Fernando Langa,*[,‡] Juan T. López Navarrete,*[,†] and Juan Casado*[,†]

[†]Department of Physical Chemistry, University of Málaga, Campus de Teatinos s/n, Málaga 29071, Spain

[‡]Instituto de Nanociencia, Nanotecnología y Materiales Moleculares (INAMOL), University of Castilla-La Mancha, Campus de la Fábrica de Armas, 45072-Toledo, Spain

Supporting Information

ABSTRACT: In going from short to large size thienylene-vinylene diferrocenyl cations, the transition from a charge delocalized to a localized state is addressed by resonance Raman spectroscopy and supported by theoretical model chemistry. The shorter members, dimer and tetramer, display conjugated structures near the cyanine limit of bond length equalization as a result of the strong interferrocene charge resonance, producing a full charge *delocalized* mixed valence system. In the longest octamer, charge resonance vanishes and the cation is *localized* at the bridge center (the mixed valence property disappears). The hexamer is at the *delocalized*-to-*localized* turning point. Solvent and variable-temperature Raman measurements highlight this borderline property. A detailed structure−property correlation of bond length alternation data and Raman frequencies is proposed to account for the whole set of spectroscopic properties, with emphasis on the changes observed with the size of the molecular wire.

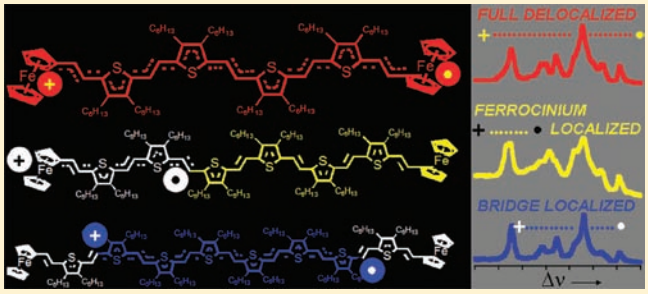

I. INTRODUCTION

Organic π−conjugated molecules are of tremendous interest due to their applications as semiconducting elements in the field of plastic electronics.[1] The understanding of the mechanisms of charge transport in these semiconductors, at any scale (molecular wire, nanoscopic, or mesoscopic), is therefore of prime importance. Organic molecules of the type M−B−M, where two equal redox centers (M) of a molecule in different oxidation states compete for the charge via a mediating molecular bridge (B), are interesting charge transfer models, or mixed valence systems (MV).[2] Many studies of M−B−M-type molecules have focused on determining electron transfer rates either by NMR[3] or ESR,[4] by IR for metal-centered molecules,[5] by means of the reorganization energies and electronic coupling by analyzing optical transitions,[6] etc.

An important aspect of symmetric M−B−M systems is the extent of the delocalization of the charge along the molecular wire. In this regard, M−B−M molecules in their singly oxidized state can be catalogued in two main types (Robin−Day classification of mixed valence systems[7]): localized systems characterized by the placement of the total charge in one of the donor groups (class II, $^{+}$M−B−M or M−B−M^{+}; see Scheme 1) and delocalized species where the charge excess fully spreads out between the two redox centers over the bridge (class III, $^{\delta+}$M−B$^{\Delta+}$−M$^{\delta+}$ in Scheme 1). The case of M−B^{+}−M represents the disappearance of mixed valence property and constitutes the possibility of the charge being exclusively localized in the bridge. The transformation or interconversion of these classes of species, in essence the localization-to-delocalization of the charge, mimics the intramolecular charge displacement, which is the paradigmatic event in the transport of the charge along a given molecular wire.[8]

Oligothiophenes represent an eminent family of organic molecules, broadly applied as bulk semiconductors and as molecular wires.[9] The stabilization of the charge in oligothiophenes is conducted by a cooperative transformation of the successive conjugated C═C/C−C bonds which accordingly modify their bond length alternation pattern (BLA, or average difference between the consecutive C═C double and C−C single bonds of the conjugated path[10]). Vibrational normal modes moving the conjugated path (i.e., C═C/C−C stretches) are thus informative of the transformation of the conjugated skeleton, and their associated bands, especially active in the Raman spectrum, are a fingerprint of the placement of the charge within the molecule, that is, of its localized or delocalized character.[11] These skeletal C═C/C−C modes are very visible in the Raman experiment because of (i) highly efficient electron−phonon coupling along these vibrational modes in conjugated molecules and (ii) resonance Raman effects when excitation is provided with a laser of the same energy of the new intragap electronic

Received: January 18, 2012
Published: March 7, 2012

dx.doi.org/10.1021/ja3005607 | J. Am. Chem. Soc. 2012, 134, 5675−5681

Scheme 1. Representation of the Three Interconverting Localized-to-Delocalized Forms in a Single Charged B−M−B Molecular Wire

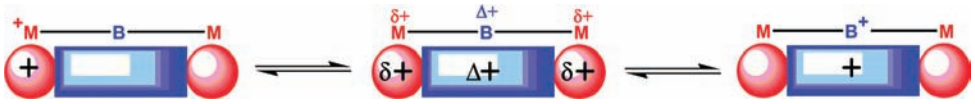

Scheme 2. Series of Fc−*m*TV−Fc and *m*TV Compounds with n = 1, 3, 5, and 7 and $m = n + 1$ (i.e., for n = 1, Fc−2TV−Fc and 2TV)

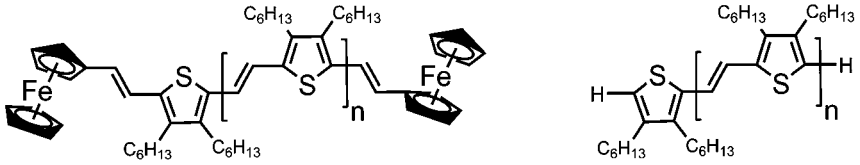

Scheme 3. Synthesis of Fc−*m*TV−Fc Compounds

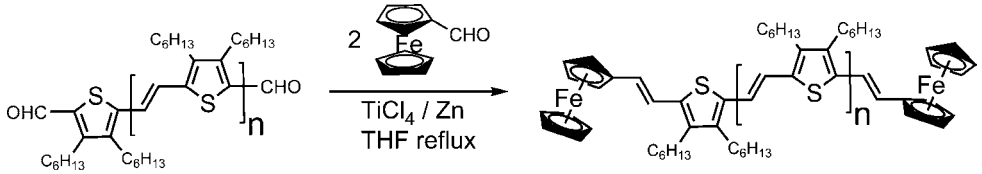

states created in the oxidized charged species (i.e., by doping). Resonance Raman spectroscopy is very valuable for chemical detection since allows one to record spectra of species at the level of traces.[12]

This work presents the preparation of a series of medium to large size oligothiophene-vinylene oligomers (Scheme 3 and Supporting Information) in which the delocalized/localized property is introduced in the radical cation state by two end-capping ferrocenes,[13] thus mimicking the M−B−M structural formula. For comparisons, the same oligothiophenes-vinylene oligomers without ferrocenes are also studied (Scheme 2). Our Raman study proposes (i) the analysis of the ground electronic state Raman frequencies of the selectively enhanced C═C/C−C Raman modes, (ii) their evolution as a function of the molecular length, (iii) the discussion in terms of localization or delocalization of the charge, and (iv) the use of theoretical chemistry input and electrochemistry to corroborate the Raman spectroscopic results.

II. EXPERIMENTAL AND THEORETICAL DETAILS

1. Synthesis. Preparation of the samples in Scheme 3 follows by McMurry cross-coupling between OHC−*m*TV−CHO and ferrocenecarboxaldehyde (see additional details in Supporting Information).[14] Oxidation of the samples was achieved by stepwise addition of $FeCl_3$ in dichloromethane followed by UV−vis−NIR absorption spectroscopy (see Supporting Information).

2. Raman Spectroscopy. All the spectra presented in this work are taken with the 1064 nm Raman excitation, corresponding to resonance Raman signatures of the radical cations as have been obtained by exciting the NIR absorption bands at 1000−1200 nm (see Figure 3 below), and 1064 nm FT−Raman spectra were measured using an FT−Raman accessory kit (FRA/106-S) of a Bruker Equinox 55 FT−IR interferometer. A continuous−wave Nd−YAG laser working at 1064 nm was employed for excitation. A germanium detector operating at liquid nitrogen temperature was used. Raman scattering radiation was collected in a back-scattering configuration with a standard spectral resolution of 4 cm^{-1}, and 1000−3000 scans were averaged for each spectrum. Temperature-variable FT-Raman measurements were performed using a variable-temperature cell Specac P/N 2100. This cell consists of a surrounding vacuum jacket (0.5 Torr), which is combined with a refrigerant Dewar and a heating block as the sample holder, allowing temperatures between −170 and 250 °C to be achieved. A Graseby Specac automatic temperature controller was employed. Samples were inserted into the Dewar/cell holder, and the spectra were recorder after waiting for thermal equilibrium of the sample.

3. UV−Vis−NIR Spectroscopy. 190−3000 nm absorption spectra were recorded with a Lambda 19 spectrophotometer from Perkin-Elmer.

4. Electrochemistry. Electrochemical experiments have been conducted in *o*-DCB/acetonitrile (4:1) at room temperature by using 0.1 M tetrabutyl ammonium perchlorate (Bu_4NClO_4) as the supporting electrolyte. A glassy carbon was used as the working electrode and a Pt wire as the auxiliary electrode against a pseudoreference electrode of Ag/0.001 M $AgNO_3$, 0.1 M Bu_4NClO_4. All redox potentials provided are referred to the Fc/Fc^+ pair.

5. Theoretical Details. The molecular geometries of the neutral and radical cation states were calculated at the Density functional theory (DFT) level using the B3LYP functional[15,16] as implemented in the Gaussian 09 program.[17] For the open-shell cations, the unrestricted method, UB3LYP, was used. The 6-31G** basis set[18−20] was chosen as a good compromise between accuracy and applicability to large molecules. The bond length alternation (BLA[10]) parameters for the thienyl rings were calculated as the difference between the length of the (C_β−C_β') bond and the average of the (C_α−C_β) and (C_α−C_β') bonds. For the vinylene goups, the BLA's were calculated as the average of the difference of the single bond distances minus the double bond ones. On the basis of the resulting ground-state optimized geometries, harmonic vibrational frequencies and Raman intensities were calculated. The final frequencies were scaled by a uniform factor of 0.96 as recommend by Scott and Radom.[21] The ionization potentials (IPs) were calculated directly from the relevant points on the potential energy surfaces using the standard procedure detailed in the literature.[22] Specifically, adiabatic IPs were evaluated as the energy difference between the relaxed cation and the neutral molecule.

III. RESULTS AND DISCUSSION

1. Nature of the Conjugational Vibrational Mode in the Raman Spectrum. The Raman frequency of the C═C vinylene stretching mode, ν_{vinyl}(C═C), is central to our discussion, as it represents the vibrational Raman probe of molecular C═C/C−C conjugation. This appears as a strong Raman

dx.doi.org/10.1021/ja3005607 | J. Am. Chem. Soc. 2012, 134, 5675−5681

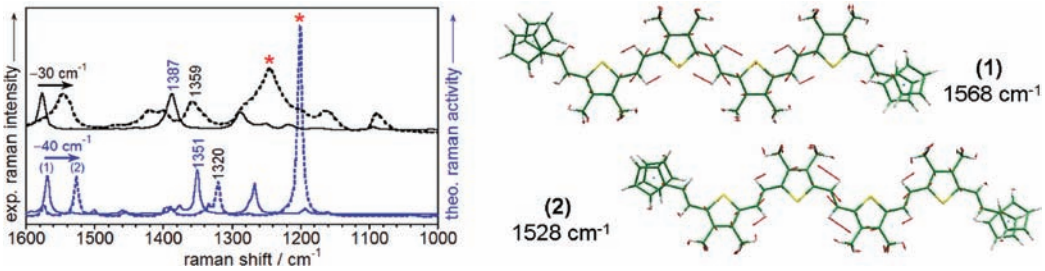

Figure 1. Experimental (top in black) and DFT/(U)B3LYP/6-31G** (bottom in blue) spectra of neutral (solid line) Fc−4TV−Fc and of its radical cation (dotted line) species together with the vibrational modes associated with the ν_{vinyl}(C═C) bands in both redox species.

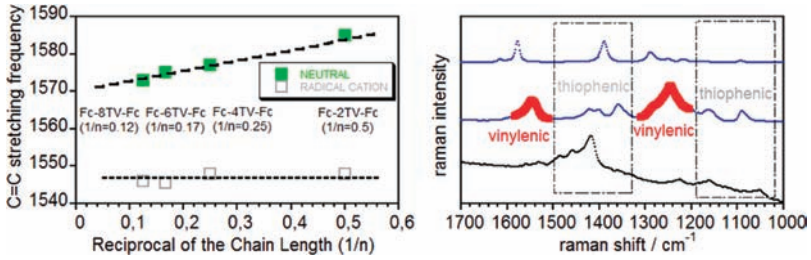

Figure 2. (Left) ν_{vinyl}(C═C) frequency behavior of Fc−*m*TV−Fc (neutral and radical cations) with the reciprocal of the chain length. (Right) FT-Raman spectra of the neutral (top) and radical cation (middle) of Fc−4TV−Fc and of the cation species of dimethyl quaterthiophene (bottom) as a representative case of pure thienyl cation. Bands in red highlight the cyanine-like vinylenic pattern.

intensity band in the 1570−1590 cm^{-1} region of the neutral Fc−*m*TV−Fc compounds: for example, in Figure 1, at 1577 cm^{-1} in neutral Fc−4TV−Fc associated with the DFT/B3LYP/6-31G** theoretical band at 1568 cm^{-1} which corresponds to a symmetric vibration mostly of the vinylene C═C stretches with an appreciable contribution of the thiophenic C═C stretches as well (Figure 1).

After one-electron extraction, the theoretical neutral ν_{vinyl}(C═C) band moves toward lower frequencies by 40 cm^{-1} and to a similar extent, by 30 cm^{-1}, in the experimental spectrum from Fc−4TV−Fc to $[Fc-4TV-Fc]^{\bullet+}$. The thiophenic bands around 1400 cm^{-1} in both redox species move similarly in the theoretical and experimental spectra (Figure 1). Interestingly, the most intense band of the cationic species is measured and predicted in the same 1200−1250 cm^{-1} interval and due to vinylenic vibrational modes (see asterisks in Figures 1 and S13, Supporting Information). In general, the coincidence between the experimental and theoretical quantities is extraordinary good taking into account the rather large molecular size and number of atoms of Fc−4TV−Fc. We will assume that this good correlation warrants the use of the theoretical molecular parameters to discuss the spectroscopic properties. In the radical cation, the vibrational normal mode of the theoretical band at 1528 cm^{-1} (experimentally at 1548 cm^{-1}) also highlights a strong vibrational mixing between the ν_{vinyl}(C═C) and $\nu_{thienyl}$(C═C) modes, significantly larger than the neutrals. This reinforces further that in order to account for the size frequency behavior of these conjugational Raman bands, either in the neutrals or in the cations, it is required to invoke its dual ν_{vinyl}(C═C) + $\nu_{thienyl}$(C═C) nature in connection with the C═C/C−C BLA's of vinylene, of thiophenes, and of the two together.

2. FT-Raman Spectra of Neutrals and Cations: Insights on the Delocalized-to-Localized Property. In Figure 2 the frequency behavior of the ν_{vinyl}(C═C) Raman band around 1540−1590 cm^{-1} is represented for the neutral and for the generated radical cation species.

This band shows a continuous frequency downshift on chain lengthening for the neutrals[23] which perfectly adjusts with the reciprocal of the chain length. This behavior is in agreement with (i) the well-known large conjugation length of *n*TV arrays[14] (i.e., much larger than in homogeneous thiophene oligomers), which indicates that our octamer conjugation is still below the conjugation length limit, and (ii) this frequency downshift being a particular feature of the thienylene-vinylene moiety with marginal involvement of the ferrocene caps. On passing from the neutral to the radical cations, a large 30−40 cm^{-1} frequency downshift is observed that is justified by the bonding nature of the C═C bonds in the HOMO orbital of the neutral systems (see Figure S12, Supporting Information) that is decreased with oxidation provoking the C═C bond weakening and consequently the Raman ν_{vinyl}(C═C) frequency downshift.[24] The Raman spectrum of $[Fc-4TV-Fc]^{\bullet+}$ presents a particular profile with two stronger bands around 1550 and 1240 cm^{-1} with major contents of vinylene modes ν_{vinyl}(C═C) and in-plane β_{vinyl}(C−H), respectively (see Figure S13, Supporting Information), or, in other words, a spectral profile dictated by the oligoene-like character imparted by the vinylene bridges.

In contrast to the neutrals, the main finding in the oxidized compounds is the frequency constancy of the ν_{vinyl}(C═C)

Scheme 4. Representation of the Cyanine Limit (full delocalized state) in a Streptocyanine

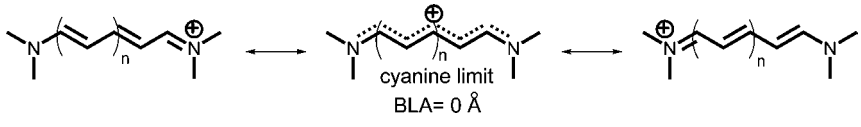

dx.doi.org/10.1021/ja3005607 | J. Am. Chem. Soc. 2012, 134, 5675−5681

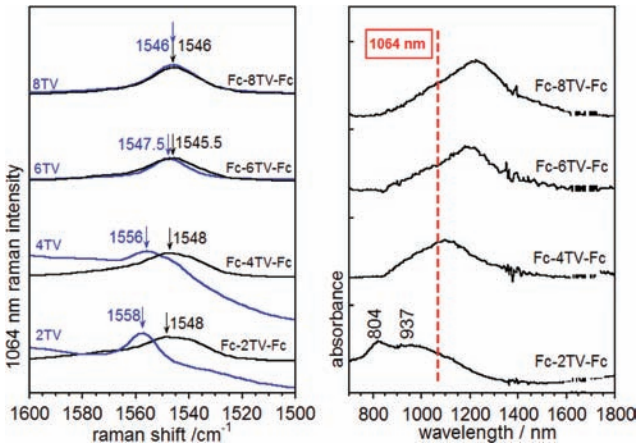

Figure 3. (Left) FT-Raman spectra of $[Fc{-}m TV{-}Fc]^{\bullet+}$ and $[m TV]^{\bullet+}$ in dichloromethane. (Right) NIR absorption spectra of $[Fc{-}m TV{-}Fc]^{\bullet+}$ samples highlighting the laser wavelength of the Raman experiment.

band, an effect now necessarily ascribed to the ferrocene caps in the context of competition for the charge through the *n*TV wire. Due to symmetry reasons, a possible mechanism to equally share the positive charge between the ferrocene donors would be the charge in resonance through the conjugated bridge. This description is similar to the case of molecules in the cyanine limit in which donor−acceptor competition produces bond length equalization and, in the ultimate case, the vanishing of the BLA pattern of the C═C/C−C conjugated path (see Scheme 4). The first consequence of this cyanine-like structural property in our cationic molecules would be the large reduction of the BLA pattern, eventually approaching bond length equalization. This structural property might certainly justify the near independence of the ν_{vinyl}(C═C) frequency with the chain length, since small BLA's would give rise to small frequency differences. Merocyanine chromophores with structures near the cyanine limit also possessing vinylene bridges, which display resonant Raman spectra, have been described in the literature, the most intense bands being around 1550 and 1230 cm^{-1} in analogy with our cases.[25] In the last section, we will provide structural insights of the cyanine-like BLA values of our diferrocenyl oligomers in connection with their associated Raman frequencies.

3. The Role of the Ferrocenes. To scrutinize in more detail the interesting resonance effect between the two ferrocene caps, the FT-Raman spectra of the $Fc{-}mTV{-}Fc$ and *m*TV cations (i.e., with a without ferrocenes) in Figure 3 are compared.

The first noticeable result is that the spectra of $[Fc{-}8TV{-}Fc]^{\bullet+}$ and $[8TV]^{\bullet+}$ display identical ν_{vinyl}(C═C) Raman profiles, meaning that the longest diferrocenyl cation does not feature interferrocene charge exchange, but conversely, it is a *pure* bridge localized species (M−B^{+}−M in Scheme 1). In contrast, the Raman spectra of the $[Fc{-}2TV{-}Fc]^{\bullet+}$/$[2TV]^{\bullet+}$, $[Fc{-}4TV{-}Fc]^{\bullet+}$/$[4TV]^{\bullet+}$, and $[Fc{-}6TV{-}Fc]^{\bullet+}$/$[6TV]^{\bullet+}$ pairs differ by 10, 8, and 2 cm^{-1}, respectively, highlighting the role of the ferrocenes. For the three shorter diferrocenyl compounds, these Raman data are consistent with the completely delocalized picture deduced by the cyanine-like behavior but revealing the decreasing role of the iron centers with the enlargement of the chain; in fact, in $[Fc{-}6TV{-}Fc]^{\bullet+}$ the small frequency difference already advertises the weak strength of the interferrocene charge resonance. Clearly, however, $[Fc{-}6TV{-}Fc]^{\bullet+}$ is the turning point of this behavior and in $[Fc{-}8TV{-}Fc]^{\bullet+}$ the charge entirely falls in the bridge. This behavior is also interpretable in terms of mixed valence theory, as it stands that for short systems full resonance and fully delocalized systems are mostly expected.

In consequence, we can formulate the following description as sketched in Scheme 5: (i) For the shorter members, oxidation produces full charge delocalized systems with cyanine-like

Scheme 5. Representation of Our Hypothesis about the Delocalized-to-Localized States of $[Fc{-}mTV{-}Fc]^{\bullet+}$

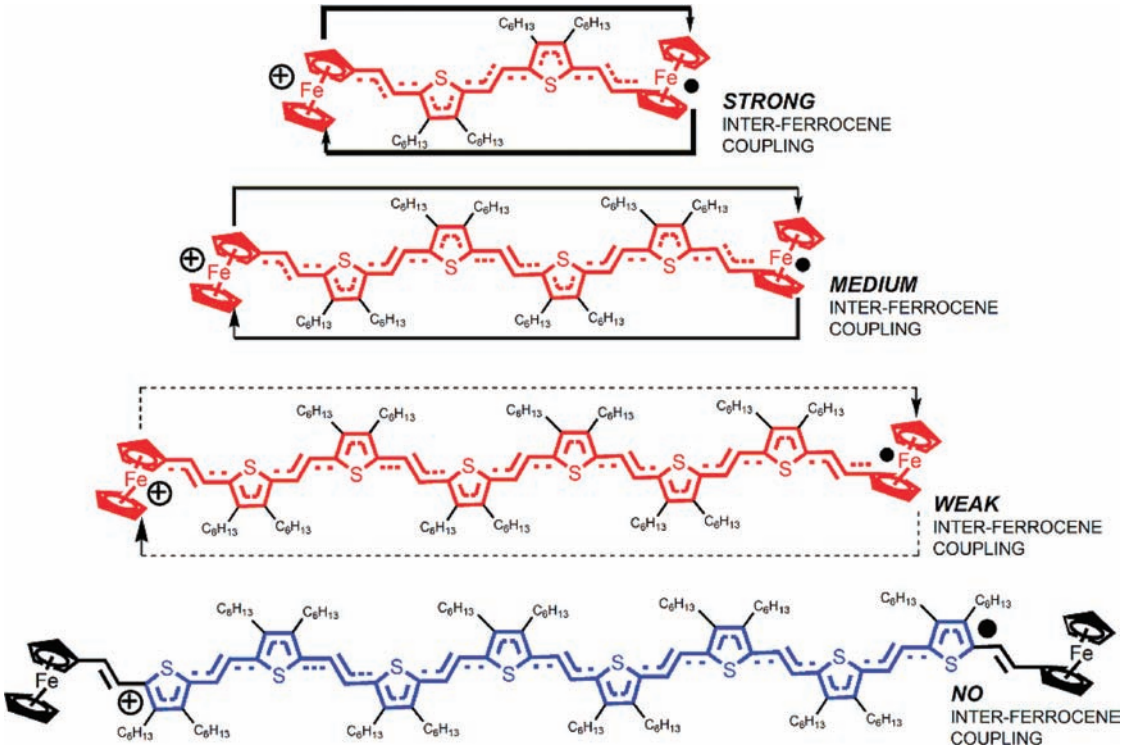

dx.doi.org/10.1021/ja3005607 | J. Am. Chem. Soc. 2012, 134, 5675−5681

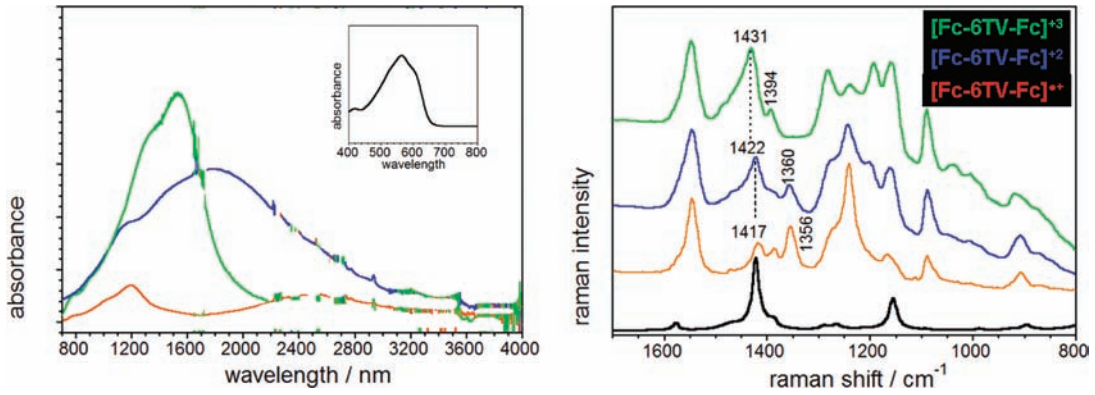

Figure 4. Vis–NIR (left) and 1064 nm Raman (right) spectra of Fc–6TV–Fc as radical cation (maroon), dication (blue), and radical trication (green). Oxidations were done with $FeCl_3$ in CH_2Cl_2 at room temperature. The inset corresponds to the UV–vis spectrum of the neutral.

properties in the vinylene and thiophene bridges. (ii) With the enlargement of the wire, the charge increasingly invades the bridge with less residence in the terminal ferrocenes. (iii) Fc–6TV–Fc is the last member where the ferrocenes take part in the stabilization of the cation. In other words, $[Fc–6TV–Fc]^{\bullet+}$ represents the transit from a delocalized species ($^{\delta+}M–B^{\Delta+}–M^{\delta+}$ in Scheme 1) to a localized one ($M–B^{+}–M$ in Scheme 1).

4. FT-Raman Spectra of Higher Oxidation States. Additional insights of the particular electronic structure of the largest system experiencing through bridge interferrocene interaction, $[Fc–6TV–Fc]^{\bullet+}$, come from their multiple cationic oxidation states. Figure 4 shows the FT-Raman spectra of Fc–6TV–Fc in its three stable oxidized states, also identified by UV–vis–NIR spectroscopy.

Posterior oxidations of the radical cation, to the dication and trication, produce the progressive disappearance of the typical two intense band pattern of the cyanine-like radical cation. Simultaneously, the thiophenic Raman bands around 1400 cm^{-1} get stronger and change their frequency in accordance with the alteration of the thienylene-vinylene structure to accommodate an increasing number of charges.[24]

5. Solvato- and Thermodependence of the Spectra. Also for $[Fc–6TV–Fc]^{\bullet+}$ we have conducted Raman solvatochromic and thermospectroscopic studies (Figure 5). In the

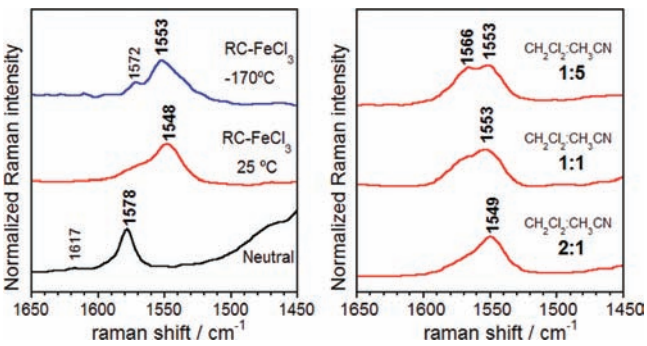

Figure 5. FT-Raman spectra of $[Fc–6TV–Fc]^{\bullet+}$ (left) at various temperatures and (right) in CH_2Cl_2:CH_3CN mixtures at room temperature.

Raman spectrum of $[Fc–6TV–Fc]^{\bullet+}$, the increasing of the polar character of the solvent produces the appearance of a new peak at 1566 cm^{-1}, which resembles that of the shorter Fc–*m*TV–Fc cations [i.e., the ν_{vinyl}(C=C) at higher frequencies], characterized by a large content of ferrocene in the resonance species. Conversely, if this new band would belong to a bridge localized state (as $[Fc–8TV–Fc]^{\bullet+}$), then the new Raman band of $[Fc–6TV–Fc]^{\bullet+}$ would resemble that of $[6TV]^{\bullet+}$, and that is not the case either.

The way to conciliate these data is by supposing that the fully delocalized interferrocene species is in equilibrium with a species that localizes the charge in one of the ferrocenes ($^{+}M–B–M$) or localized ferrocenium species, delineating the collapse of the interferrocene coupling due to the already weak interaction in the delocalized $[Fc–6TV–Fc]^{\bullet+}$. Nonetheless, the two peaks simultaneously appear in the spectrum in the polar solvent emphasizing the equilibrium between the ferrocenium localized and the fully delocalized forms, such as represented in Scheme 6. In essence, this is highlighting a molecule able to convert between localized and delocalized states or borderline class II/class III in the context of the mixed valence theory.

On the other hand, cooling $[Fc–6TV–Fc]^{\bullet+}$ to −170 °C also produces the resolution of a high-energy component at 1572 cm^{-1}. These changes are also interpretable in similar terms as those in polar media although the displacement of the localized/delocalized equilibrium is only moderate.

6. Electrochemical Properties in the Delocalized/Localized Context. It is now pertinent to understand the electrochemical properties of the samples, summarized in Table 1, in the light of the previous Raman spectroscopic results. Oxidation of the diferrocenyl samples appears at lower potentials, compared with the unsubstituted analogues, as a result of the ferrocene resonance stabilization. On the other hand, oxidation potentials decrease with the enlargement of the bridge due to the increasing participation of the bridge in the charge resonance. For the same reason the oxidations potentials of *m*TV and Fc–*m*TV–Fc get more similar for the largest compounds. The shorter compounds display simultaneous two-electron extractions, indicating that the divalent species are more stable than the radical cations that could be a consequence of the highly *polar* properties of the electrochemical medium (i.e., note that the polarity of the medium provokes the localization of the charge in one ferrocene).

The estimated ionization potentials (IPs) calculated at both Koopman's theorem (KT)[26] and self-consistent field (ΔSCF) levels are also collected in Table 1. It is found that HOMO destabilizes from the dimer to the hexamer, and smaller IP values are found, while the values are nearly constant from the hexamer to the octamer. In agreement with the higher oxidation potentials obtained for the unsubstituted *m*TV molecules, larger IPs and more stabilized HOMOs are found for these in comparison with their diferrocenyl anologues. The HOMO

dx.doi.org/10.1021/ja3005607 | J. Am. Chem. Soc. 2012, 134, 5675–5681

Scheme 6. Delocalized to Localized Equilibrium in $[Fc-6TV-Fc]^{\bullet+}$

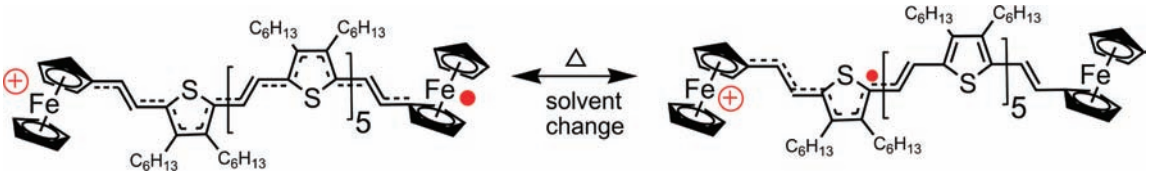

Table 1. Redox Potentials (versus Fc/Fc^{+}) of the Studied Compounds in *o*-DCB/Acetonitrile (4:1) with 0.1 M Bu_4NClO_4[a]

				calcd values	
	E^1_{ox}	E^2_{ox}	E^3_{ox}	Koopmans[d]	$IP_{adiabatic}$[e]
Fc−2TV−Fc	0.05[b]	0.41	0.80	4.47	5.29
Fc−4TV−Fc	0.03[b]	0.16	0.40	4.30	4.99
Fc−6TV−Fc	0.03[b]	0.09	0.20	4.22	4.83
Fc−8TV−Fc	0.05[c]	0.31	0.64	4.20	4.72
2TV[f]	0.28	0.59		4.93	6.26
4TV[f]	0.15	0.33		4.43	5.32
8TV[f]	0.04[c]		0.34	4.23	4.81

[a]Working electrode, carbon glassy disk; counter electrode, Pt wire; pseudoreference, Ag/0.001 M $AgNO_3$, 0.1 M Bu_4NClO_4. [b]Two-electron oxidation process. [c]Four-electron oxidation process. [d]Values according to the Koopsman theorem in ref 26. [e]Calculated first ionization potentials (IPs) for isolated Fc−*m*TV−Fc and *m*TV molecules obtained from ΔSCF at the B3LYP/6-31G** level. [f]Data from ref 14b.

wave functions are completely delocalized between the ferrocenes through the TV bridge in line with the formation of fully delocalized systems for the shorter members of the series while the HOMO of Fc−8TV−Fc is bridge-localized (see topologies in Figure S12, Supporting Information).

7. Theoretical Model Chemistry. DFT//(U)B3LYP/6-31G** bond length alternation parameters (i.e., BLA) of the thienyl rings and of vinylene groups of the Fc−*m*TV−Fc compounds together with the average value of the two are represented in Figure 6. For the neutrals, the enlargement of the chain provokes a lowering of the BLA values in the two classes of alternating moieties with the increment of TV units at the origin of the downshift of the $\nu_{vinyl}(C{=}C)$ frequency and in line with the well-known close relationship between increased conjugation and BLA contraction.[27] It must be noted that it is the simultaneous decrease of the vinylene and of the thienylene BLA's (and therefore of its average value) that provokes the 1570−1580 cm^{-1} Raman frequency downshift due to its dual and collective $\nu_{vinyl}(C{=}C) + \nu_{thienyl}(C{=}C)$ character.

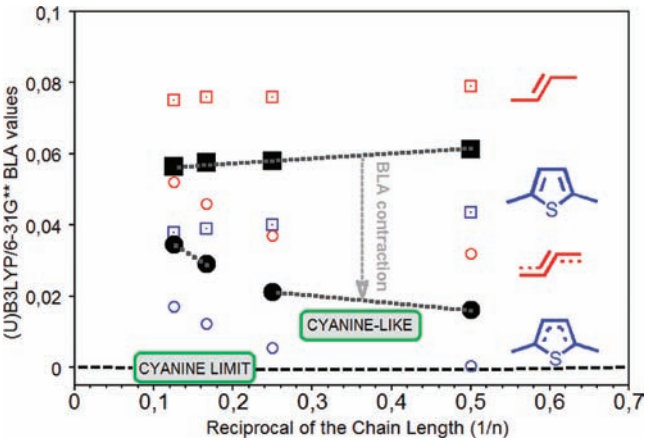

Figure 6. B3LYP/6-31G** BLA's in angstroms for the vinylene (red squares) and thiophene (blue squares) moieties and the average value of the two (black squares) for the neutral compounds. (U)B3LYP/6-31G** BLA's in angstroms for the vinylene (red circles) and thiophene (blue circles) moieties and the average value of the two (black circles) for the cations. These data are represented versus the reciprocal of the number of TV units.

For both vinylene and thiophene groups, oxidation significantly diminishes their BLA values, in agreement with the large ≈30−40 cm^{-1} Raman frequency downshift observed in the spectra from the neutral to the radical cations. The magnitude of the BLA contraction decreases with the enlargement of the chain length, which is directly related with the reduction of the difference of the $\nu_{vinyl}(C{=}C)$ frequencies between the neutrals and cations with the chain length (for instance, 38 cm^{-1} in Fc−2TV−Fc and 27 cm^{-1} in Fc−8TV−Fc). It is observed in Figure 6 that for the radical cations of the two shorter members, the overall BLA's are clearly lower; in particular, for the thiophenes their BLA's are just in the cyanine limit border while for the vinylenes these are larger, resulting in a overall structural BLA that slightly separates from the cyanine limit but still remains close to it, highlighting a cyanine-like pattern. All in all, these data indicate that $[Fc-2TV-Fc]^{\bullet+}$ and $[Fc-4TV-Fc]^{\bullet+}$ can be catalogued as cyanine-like dyes, with similar BLA's that would account for the equal 1548 cm^{-1} Raman frequency in the two shorter cations. For the octamer cation, the BLA's are comparatively large, possibly revealing a marked difference between the geometries of the moieties where the charge resides (molecular center) and the terminal sides of the *n*TV array that the charge leaves almost unaltered due to the inactivity of the ferrocenes. As far as the BLA's values are concerned, $[Fc-6TV-Fc]^{\bullet+}$ is placed in a transitional stage between fully delocalized cyanine-like behavior and a bridge-localized situation. The similitude between the $[Fc-6TV-Fc]^{\bullet+}$ and $[Fc-8TV-Fc]^{\bullet+}$ $\nu_{vinyl}(C{=}C)$ frequencies would result from different effects that contribute in the same direction, that is, the larger number of *n*TV units in $[Fc-8TV-Fc]^{\bullet+}$ (which favors π−electron delocalization) and the interferrocene coupling that extends resonantly charge delocalization in $[Fc-6TV-Fc]^{\bullet+}$. The lowest $\nu_{vinyl}(C{=}C)$ frequency of 1545.5 cm^{-1} for this hexamer could highlight the largest distance of delocalization of the charge, which spreads over the entire C=C/C−C conjugated path from one ferrocene to the other. As a last insight of relevance, theoretical results allow us to estimate molecular distances in $[Fc-6TV-Fc]^{\bullet+}$ revealing that interferrocene coupling takes place for distances of about 38 Å.

IV. CONCLUSIONS

We have addressed the analysis of the transition of the positive charge from a localized to a delocalized state in radical cations of thienylene-vinylene diferrocenyl oligomers of variable length by means of the analysis of the frequencies of the resonantly

dx.doi.org/10.1021/ja3005607 | J. Am. Chem. Soc. 2012, 134, 5675−5681

enhanced ν_{vinyl}(C=C) Raman modes. We have shown that the case of $[Fc-6TV-Fc]^{\bullet+}$ is at the turning point between the two limiting structures, which is corroborated by tuning the localized-to-delocalized equilibrium with the modification of the solvent and the temperature. These radical cations feature cyanine-like delocalized systems due to efficient interferrocene coupling which, in addition, is modulated by the length of the bridge. It is concluded from this analysis that thienylene-vinylene spacers, owing to their outstanding conjugative properties, are excellent candidates to unimolecularly transport electronic stimuli between distant electrogenerating centers (i.e., metallic electrodes or nanoparticles). The performance of thienylene-vinylene bridges as molecular wires is highlighted by their ability to transmit the interferrocene coupling over distances near 40 Å, which is an outstanding wirelike feature.

■ ASSOCIATED CONTENT

Supporting Information

Chemical characterization, electronic absorption and Raman spectra, orbital topologies, and vibrational normal modes, together with additional and theoretical data. This material is available free of charge via the Internet at http://pubs.acs.org.

■ AUTHOR INFORMATION

Corresponding Author

casado@uma.es

Notes

The authors declare no competing financial interest.

■ ACKNOWLEDGMENTS

This work was supported by the Ministerio de Educación y Ciencia (MEC) of Spain by projects CTQ2009-10098, CTQ2010-17498, and HOPE CSD2007-00007 and by the Junta de Andalucía by the research project PO9-4708. S.R.G. thanks the Junta de Andalucía for a personal doctoral grant. M.C.R.D. is grateful to MICINN for a "Ramón y Cajal" research contract.

■ REFERENCES

(1) (a) James, D. K.; Tour, J. M. *Chem. Mater.* **2004**, *16*, 4423. (b) Klauk, H. *Chem. Soc. Rev.* **2010**, *39*, 2643. (c) Perepichka, D. F.; Meng, H.; Wuld, F. *Adv. Mater.* **2005**, *17*, 2281. (d) Allard, S.; Foster, M.; Souharce, B.; Thiem, H.; Scherf, U. *Angew. Chem. Int. Ed.* **2008**, *47*, 4070. (e) Melzer, C.; Von Seggern, H. *Nat. Mater.* **2010**, *9*, 470.

(2) (a) Hush, N. S. *Prog. Inorg. Chem.* **1967**, *8*, 391. (b) Marcus, R. A.; Sutin, N. *Biochim. Biophys. Acta* **1985**, *811*, 26. (c) Hoekstra, R. M.; Telo, J. P.; Wu, Q.; Stephenson, R. M.; Nelsen, S. F.; Zink, J. I. *J. Am. Chem. Soc.* **1997**, *119*, 10213. (d) Bixon, M.; Joner, J. *Adv. Chem. Phys.* **1999**, *106*, 35. (e) D'Alessandro, D. M.; Keene, F. R. *Chem. Soc. Rev.* **2006**, *35*, 424. (f) Hankache, J.; Wenger, O. S. *Chem. Rev.* **2011**, *111*, 5138. (g) Heckmann, A.; Lambert, C. *Angew. Chem. Int. Ed.* **2012**, *51*, 326.

(3) (a) de Boer, E.; MacLean, C. J. *Chem. Phys.* **1966**, *44*, 1334. (b) Elliot, C. M.; Derr, D. L.; Matyushov, D. V.; Newton, M. D. *J. Am. Chem. Soc.* **1998**, *120*, 11714.

(4) (a) Heinen, U.; Berthold, T.; Kothe, G.; Stavitski, E.; Galili, T; Levanon, H.; Wiederrecht, G.; Wasielewski, M. R. *J. Phys. Chem. A* **2002**, *106*, 1933. (b) Nelsen, S. F.; Ismagilov, R. F.; Gentile, K. E.; Powell, D. R. *J. Am. Chem. Soc.* **1997**, *119*, 10213.

(5) (a) Ito, T.; Hamaguchi, T.; Nagino, H.; Yamaguchi, T.; Washington, J.; Kubiak, C. P. *Science* **1997**, *277*, 660. (b) Demadis, K. D.; Hartshorn, C. M.; Meyer, T. J. *Chem. Rev.* **2001**, *101*, 2655.

(6) (a) Coropceanu, V.; Cornil, J.; da Silva Filho, D. A.; Oliver, Y.; Silbey, R.; Brédas, J.-L. *Chem. Rev.* **2007**, *107*, 926. (b) Heckmann, A.; Amthor, S.; Lambert, C. *Chem. Commun.* **2006**, 2959.

(7) Robin, M. B.; Day, P. *Adv. Inorg. Chem. Radiochem.* **1967**, *10*, 247.

(8) (a) Brunschwig, B. S.; Creutz, C.; Sutin, N. *Chem. Soc. Rev.* **2002**, *31*, 168. (b) Lacroix, J. C.; Chane-Ching, K. I.; Maquére, F.; Maurel, F. *J. Am. Chem. Soc.* **2006**, *128*, 7264. (c) Lambert, C.; Nöll, G.; Schelter, J. *Nat. Mater.* **2002**, *1*, 69. (d) Nelsen, S. F.; Konradsson, A. E.; Telo, J. P. *J. Am. Chem. Soc.* **2005**, *127*, 920.

(9) (a) Mishra, A.; Ma, C.-Q.; Bäuerle, P. *Chem. Rev.* **2009**, *109*, 1141. (b) Perepichka, I. F.; Perepichka, D. F.; Meng, H.; Wuld, F. *Adv. Mater.* **2005**, *17*, 2281. (c) Roncali, J. *Chem. Rev.* **1997**, *97*, 173. (d) *Handbook of Thiophene-Based Materials. Applications in Organic Electronics and Photonics*; Perepichka, I. F., Perepichka, D. F., Eds.; Wiley: Chichester, 2009.

(10) (a) Brédas, J.-L. *J. Chem. Phys.* **1985**, *82*, 3808. (b) Brédas, J.-L.; Themans, B.; Fripiat, J. P.; André, J. M.; Chance, R. R. *Phys. Rev. B* **1984**, *29*, 6761. (c) Cammi, R.; Mennucci, B.; Tomasi, B, J. *J. Am. Chem. Soc.* **1994**, *116*, 2619.

(11) (a) Castiglioni, C.; Zoppoi, M.; Zerbi, G. *J. Raman Spectrosc.* **1993**, *24*, 485. (b) Castiglioni, C.; Tommasini, M.; Zerbi, G. *Philos. Trans. R. Soc. London A* **2004**, *362*, 2425.

(12) *The Raman Effect: A Unified Treatment of the Theory of Raman Scattering by Molecules*; Long, A. D., Ed.; John Wiley & Sons: West Sussex, England, 2002.

(13) (a) Josowics, M.; Tolber, L. M. *J. Am. Chem. Soc.* **2010**, *132*, 10374. (b) Tolbert, L. M.; Zhao, X.; Ding, Y.; Bottomley, L. A. *J. Am. Chem. Soc.* **1995**, *117*, 12891. (c) Casado, J.; Rodríguez González, S.; Ruiz Delgado, M. C.; Moreno Oliva, M.; López Navarrete, J. T.; Caballero, R.; de la Cruz, P.; Langa, F. *Chem.—Eur. J.* **2009**, *15*, 2548.

(14) (a) Roncali, J. *Acc. Chem. Res.* **2000**, *33*, 147. (b) Jestin, I.; Frère, I. P.; Blanchard, P.; Roncali, J. *Angew. Chem., Int. Ed.* **1998**, *37*, 942. (c) Oswald, F.; Shafiqul Islam, D.-M.; Araki, Y.; Troiani, V.; de la Cruz, P.; Moreno, A.; Ito, O.; Langa, F. *Chem.—Eur. J.* **2007**, *13*, 3924.

(15) Becke, A. D. *J. Chem. Phys.* **1993**, *98*, 5648.

(16) Lee, C. T.; Yang, W. T.; Parr, R. G. *Phys. Rev. B* **1988**, *37*, 785.

(17) Frisch, M. J., et al.; *Gaussian 09, Revision A.02*; Gaussian, Inc.: Wallingford CT, 2009.

(18) Harihara, P. C.; Pople, J. A. *Theor. Chim. Acta* **1973**, *28*, 213.

(19) Hehre, W. J.; Ditchfield, R.; Pople, J. A. *J. Chem. Phys.* **1972**, *56*, 2257.

(20) Francl, M. M.; Pietro, W. J.; Hehre, W. J.; Binkley, J. S.; Gordon, M. S.; Defrees, D. J.; Pople, J. A. *J. Chem. Phys.* **1982**, *77*, 3654.

(21) Scott, A. P.; Radom, L. J. *Phys. Chem.* **1996**, *100*, 16502.

(22) Brédas, J. L.; Beljonne, D.; Coropceanu, V.; Cornil. *J. Chem. Rev.* **2004**, *104*, 4971.

(23) Hernández, V.; Casado, J.; Ramírez, F. J.; Zotti, G.; Hotta, S.; López Navarrete, J. T. *J. Chem. Phys.* **1996**, *104*, 9271.

(24) (a) Casado, J.; Hernández, V.; Hotta, S.; López Navarrete, J. T. *J. Chem. Phys.* **1998**, *109*, 10419. (b) Casado, J.; Hernández, V.; Hotta, S.; López Navarrete, J. T. *Adv. Mater.* **1998**, *10*, 1458. (c) Casado, J.; Takimiya, K.; Otsubo, T.; Ramírez, F. J.; Quirante, J. J.; Ponce Ortiz, R.; Rodríguez González, S.; Moreno Oliva, M.; López Navarrete, J. T. *J. Am. Chem. Soc.* **2008**, *130*, 14028. (d) Casado, J.; Hernández, V.; López Navarrete, J. T.; Viruela, P. M.; Ortí, E.; Takimiya, K.; Otsubo, T. *Angew. Chem., Int. Ed.* **2007**, *46*, 9057.

(25) Leng, W.; Würthner, F.; Meyers Kelly, A. *J. Phys. Chem. A* **2005**, *109*, 1570.

(26) Koopmans, T. *Physica* **1934**, *1*, 101.

(27) Casado, J.; Hernández, V.; Ruiz Delgado, M. C.; Ponce Ortiz, R; López Navarrete, J. T.; Facchetti, J. A.; Marks, T. *J. Am. Chem. Soc.* **2005**, *127*, 13364.